# Defect emission and optical gain in $SiC_xO_y$:H films

**Zhenxu Lin[a,*], Hongfei Li[b,*], Rui Huang[a,†], Yi Zhang[a], Jie Song[a], Hongliang Li[a], Yanqing Guo[a], Chao Song[a], and John Robertson[b]**

*1.School of Materials Science and Engineering, Hanshan Normal University, Chaozhou, Guangdong 521041, China*

*2.Department of Engineering, University of Cambridge, Cambridge, UK*

* These authors contributed equally to this paper

*† E-mail: rhuang@hstc.edu.cn*

**Abstract:**

Luminescent $SiC_xO_y$:H films，which are fabricated at different $CH_4$ flow rates using very high-frequency plasma-enhanced chemical vapor deposition technique, exhibit strong photoluminescence (PL) with tuning from near-infrared to orange regions. The PL features an excitation wavelength independent recombination dynamic. The silicon dangling bond (DB) defects identified by electron paramagnetic resonance spectra are found to play a key role in the PL behavior. The first-principles calculation shows that the Si DB defects introduce a mid-gap state in the band gap, which is in good agreement with the PL energy. Moreover, the band gap of a-$SiC_xO_y$:H is found to be mainly determined by Si and C atoms. Thus, the strong light emission is ascribed from the recombination of excited electrons and holes in Si DB defects, while the tunable light emission of the films is attributed to the substitution of stronger Si–C bonds for weak Si–Si bonds. It is also found that the light emission intensity shows a superlinear dependence on the pump intensity. Interestingly, the film exhibits a net optical gain under ultraviolet excitation. The gain coefficient is 53.5$cm^{-1}$ under a pumping power density of 553mW $cm^{-2}$. The present results demonstrate that the $SiC_xO_y$ system can be a very competitive candidate in the applications of photonics and optoelectronics.

***Keyword:*** Silicon oxycarbide, Defect, Photoluminescence, Optical gain

## 1. Introduction

The development of Si-based luminescent materials is motivated by the demand for cheap and complementary metal-oxide semiconductor (CMOS) light sources that are compatible with on-chip optical interconnect. Progress has been recently made in

understanding and optimizing light emission from Si-based materials, such as $SiO_x$, $SiN_x$, and $SiN_xO_y$ [1-11]. A breakthrough in this field is the realization of optical gain and light amplification from $SiO_x$-based material. Owing to the difficulty of electrical injection in wide band gap $SiO_x$ [2], silicon dioxide is commonly replaced with silicon nitride as a promising luminescent material for efficient electrical excitation [12-14]. Compared with silicon nitride, however, silicon oxynitride more effectively improves equivalent carrier injections in LEDs, thus significantly increasing the probability of carrier recombination [15, 16]. Extensive studies have recently focused on dielectric silicon oxycarbide ($SiC_xO_y$) due to its efficient light emission and applicability in Si chips. $SiC_xO_y$, which is widely used as an interlayer dielectric to reduce parasitic capacitance and resistance capacitance (RC) delay in Si chips, generally features strong white light emission [17-19]. Moreover, a $SiC_xO_y$ host matrix provides a remarkably higher solid solubility for rare earths, such as Eu and Er, compared with $SiO_2$ [20, 21]. In addition, the $SiC_xO_y$ matrix can also be used as donor that contributes to the light emission of $Eu^{2+}$ ions via energy transfer [22]. So far, defect states, such as C-related oxygen vacancies (C-NOVs), Si-NOVs, and Si-related oxygen deficiency centers, have been proposed to demonstrate the PL mechanism in $SiC_xO_y$ [23-25]. Nikas *et al* recently reported that white luminescence results from the recombination of carriers between energy bands and their tail states associated with the Si–O–C and /or Si–C bonds [26]. Although considerable effort has been devoted to understanding PL characters in $SiC_xO_y$, the origin of PL remains contradictory because of complicated Si phase structures, such as Si, SiC, and $SiO_x$, which coexist in $SiC_xO_y$. In addition, orange to near-infrared emitters that are based on silicon oxycarbide are still far from being established. In particular, the optical gain in a-$SiC_xO_y$ has never been studied.

In this work, we report on strong orange to near-infrared switching PL and net optical gain in $SiC_xO_y$:H film. The silicon dangling bond (DB) defects identified by electron paramagnetic resonance spectra are found to play a key role in the PL behavior. The first-principles calculation shows that the Si DB defects introduce a mid-gap state in the band gap. Moreover, the band gap of a-$SiC_xO_y$:H is found to be mainly determined by Si and C atoms. The origin of PL is discussed and a three-level-luminescence model is proposed to illustrate the PL and optical gain in a-$SiC_xO_y$ films.

## 2. Samples and experimental details

Amorphous silicon oxycarbide films were prepared on Si wafers and quartz via VHF-PECVD technique. $SiH_4$, $O_2$, and $CH_4$ were used as the reactant gas sources. The flow rates of $SiH_4$ and $O_2$ were maintained at 3.5 and 1.2 sccm, respectively, whereas the flow rates of $CH_4$ varied from 5 to 20 sccm. The as-deposited films were designated as Sx(x = 1, 2, 3, 4) with the flow rates of 5, 10, 15, and 20 sccm During deposition, the radio frequency power, chamber pressure, and substrate temperature were 30 W, 20 Pa, and 250 °C, respectively. The as-deposited films were also dehydrogenated at 400 °C for 1 h, and then annealed at 500 °C for 1 h in a conventional furnace under a nitrogen atmosphere. PL measurements were taken on a Jobin Yvon fluorolog-3 spectrophotometer. The band gaps of the films were determined from transmittance measurements, which were obtained with a Shimadzu UV-3600 spectrophotometer. The chemical compositions of Si, C, and O were determined by XPS. The microstructures of the films were characterized with a JEOL high-resolution TEM. The local atomic environment and bonding configuration within the films were recorded using FTIR spectroscopy. The paramagnetic defects in the films were analyzed with EPR measurements. The $SiN_x$/a-$SiC_xO_y$/$SiO_2$ strip-loading waveguide with 30 μm wide and 1cm long was fabricated on quartz. Optical gain was measured by the standard VSL technique. The sX hybrid functional was also used to calculate the band properties of SiCO systems, as well as the involved point defect.

The DFT simulations were performed using the CASTEP plane wave pseudopotential code. The norm conserving pseudopotential was used with the cutoff energy of 750eV in all calculations. The amorphous $SiC_xO_y$ structures were calculated by the GGA exchange correlational function with the Gamma point scheme due to a large supercell. The screened exchange hybrid functional was applied in all electronic property calculations to correct the well-known band gap error and provide the correct electron localization distribution. The amorphous SiCO models were generated by the first principles molecular dynamics (MD) method according the following steps: first, the system with a given ratio of Si, C, and O atoms underwent a high-temperature melting process at 2500 K for 10ps. Second, the system was then gradually cooled down to 300 K at the quenching rate of 100K/ps. Third, a rough geometry optimization was applied and H atoms were included to passivate the remaining dangling bonds (DB) on Si and C atoms. Finally, an accurate geometry optimization was performed until the residual force on each atom was lower than 0.01eV/Å.

## 3. Results and discussion

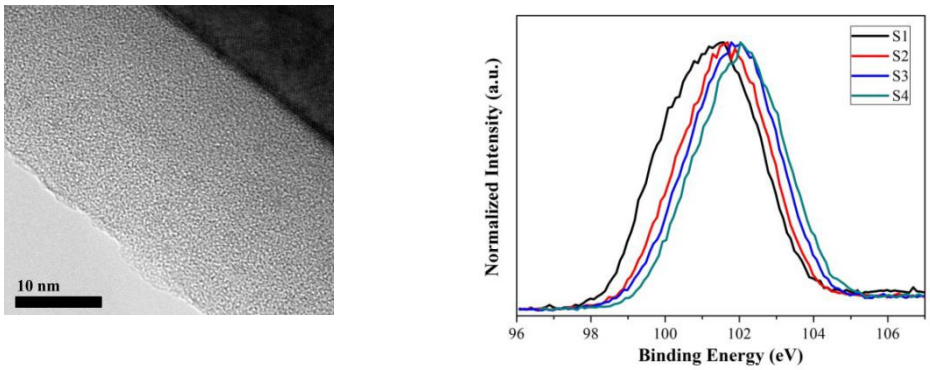


Fig. 1. (a) The cross-sectional high-resolution TEM image of the S2. (b) The Si 2*p* XPS spectra for S1, S2, S3, and S4.

The film microstructure was analyzed with high-resolution TEM (HRTEM). Fig. 1(a) presents the cross-section HRTEM image of S2. S2 does not show any sharply contrasting structures, which clearly indicates that no Si or SiC nanostructures exist in the film and that the film is amorphous. The Si 2p core level spectra of the films (Fig. 1(b)), which indicate the coexistence of different ionic states of Si atoms, were analyzed to gain more insight on phase structures in the films. The binding energy of the Si 2p peak is 101.5eV for S1, which was grown at a $CH_4$ flow rate of 5 sccm. The binding energy gradually increased to 102.1eV as the $CH_4$ flow rate increased to 20 sccm. The binding energy of the Si 2p peak for all the films is higher than that of SiC (100.8 eV) and lower than that of $SiO_2$ (103.2 eV)[27]. These results indicate that the $SiC_xO_y$ phase is the dominant phase in the films.

Fig. 2(a) shows the room-temperature PL spectra of the as-deposited $SiC_xO_y$ film grown at different $CH_4$ flow rates. The PL emission band gradually blueshifts from 735 nm to 630 nm as $CH_4$ flow rate increases from 5 to 20 sccm. Moreover, PL intensity is enhanced. Increasing the $CH_4$ flow rate to 20 sccm significantly increases the integrated PL intensity by more than two orders of magnitude compared with the PL intensity of the film grown at the $CH_4$ flow rate of 5 sccm. Interestingly, the tunable light emissions are visible to the naked eye in a bright room even at an excitation wavelength of 325 nm from a Xe lamp (Fig. 2 (b)). The tunable light emission from a–$SiC_xO_y$ can be controlled by modulating the $CH_4$ flow rate. Fig. 2(c) shows that that the PL peak positions for all the films are almost independent of excitation wavelengths. Meanwhile, the FWHM of the PL spectra for all the films almost do not widen as the excitation wavelength decreases from 375 nm to 275 nm (Fig. 2(d)). These phenomena are completely different from that observed PL that is governed by the band tail states recombination mechanism[28]. In that mechanism, the FWHM of PL gradually widens with the decrease of the excitation wavelength. These results indicate that the PL in our case may result from defect-related luminescence centers.

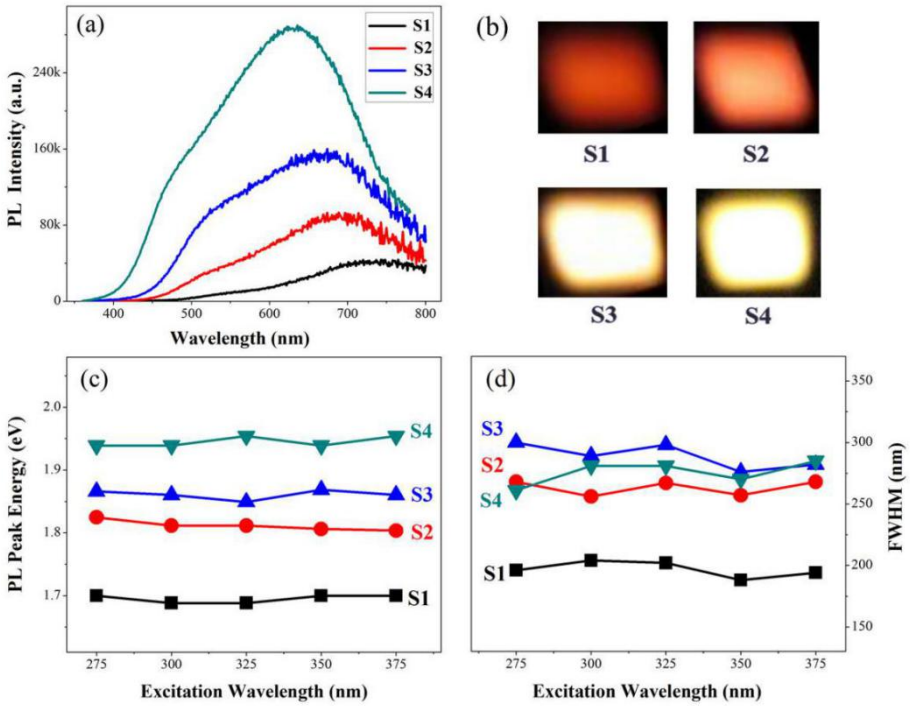


Fig. 2. (a) PL spectra of $SiC_xO_y$ films grown at different $CH_4$ flow rates: 5sccm (S1), 10sccm (S2), 15sccm (S3) and 20sccm (S4). (b) Light-emitting photos from the films under an excitation wavelength of 325 nm from Xe lamp.(c) PL peak energy versus the excitation wavelength for S1, S2, S3, and S4, (d) The full wide at half of maximum (FWHM) of the PL band excited at different wavelengths for S1, S2, S3, and S4.

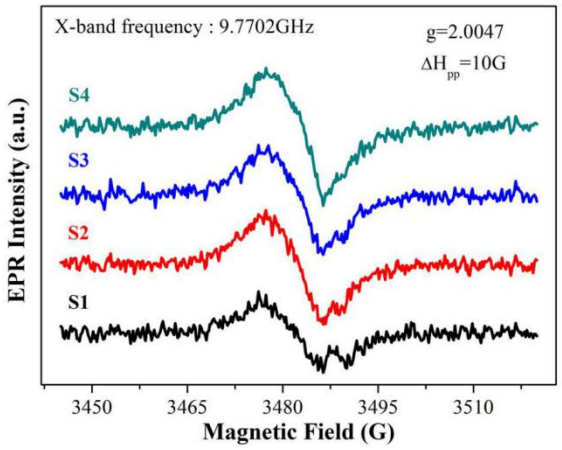


Fig. 3. Room temperature EPR spectra of the films fabricated with different $CH_4$ flow rates.

The EPR spectra (Fig. 3) of the films were examined to gain more insight on the origin of PL from a–$SiC_xO_y$ films. The g value of the EPR signal from the films can be calculated according to $g\mu BH=hv$, where $\mu B$, H, h and v is the Bohr magnetron, the spin Hamiltonian, Planck's constant and the X band frequency, respectively[29]. The spectra for all the films exhibit an EPR signal with the same g value of 2.0047 and the same line width $\triangle H_{pp}$ of approximately 10 G, which is assigned to unpaired silicon

DB defects[30]. These characteristics confirm the existence of Si DB defects in the films. As the $CH_4$ flow rate increases from 5 to 20 sccm, the integrated EPR signal intensity, which is proportional to the calculated concentration *N*s of the Si DB defects, gradually increases from $1.17\times10^{19}$ $cm^{-3}$ to $2.19\times10^{19}$ $cm^{-3}$. Therefore, the increase in PL with increasing $CH_4$ flow rates likely originated from the increased concentration of Si DB defects. To confirm this hypothesis, S2 was annealed at 500 ºC for 1 h in a conventional furnace under a nitrogen atmosphere. Fig. 4 shows the PL spectra of the as-deposited S2 and the S2 annealed at 500 ºC in $N_2$. The PL positions of the two samples do not noticeably change. However, the PL intensity of the annealed S2 is significantly enhanced by more than twice compared with that of S2. The Fig. 4 inset shows that thermal annealing at 500 ºC also remarkably enhanced the EPR signal with the same g value of 2.0047 and the same line width $\triangle H_{pp}$ of approximately 10 G as that of S2. Based on EPR results, the concentration of unpaired Si DB defects of the annealed S2 is increased by two-fold compared with that of S2, as revealed in Fig. 4 inset. This change is similar to that of PL intensity. Thus, the enhanced PL of the annealed film resulted from the increased concentration of Si DB defects. It is well known that the annealing process in $N_2$ ambient induces the diffusion of nitrogen atoms inside the film, and then the nitrogen atom will replace the Si in the network to form Si-N bonds and leave a new dangling bond, which may explain the increased concentration of Si DB defects after annealing treatment. However, the nitridation of $SiC_xO_y$ film is unlikely to occur at 500 ºC because this annealing temperature is not enough to decompose the $N_2$ gaseous molecules.

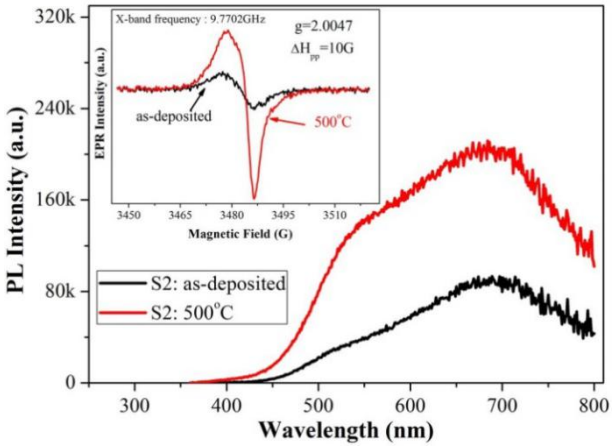


Fig.4. PL spectra of the S2 and the S2 annealed at 500 ºC in $N_2$. Inset shows the corresponding EPR spectra.

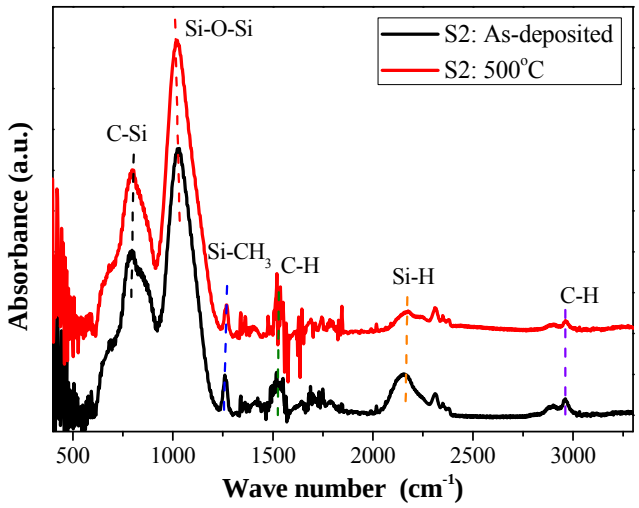


Fig.5. FTIR spectra of the S2 and the S2 annealed at 500℃.

Fig. 5 shows the FTIR absorption spectra of S2 and the annealed S2. The S2 spectrum shows the following absorption bands: two strong absorption bands at 800 $cm^{-1}$ and 1020 $cm^{-1}$, which are attributed to the C–Si and Si–O–Si stretching vibration modes, respectively[31, 32]. In addition to the above two bands, a weak band at 1260 $cm^{-1}$ is ascribed to the Si–$CH_3$ stretching vibration mode [33]. The 1520 and 2950 $cm^{-1}$ bands result from the C–H bending and stretching vibration band, respectively [33]. The 2150 $cm^{-1}$ band is due to the stretching mode of Si–H bonds [34]. A remarkable feature in the FTIR spectra (Fig. 5) is that the signal of Si–H stretching vibration band decreased after annealing at 500 ºC. This result implies that the Si–H bonds were broken and that numerous silicon dangling bonds formed during the annealing process. Therefore, the increased concentration of Si DB defects can be attributed to broken Si–H bonds, which significantly increased after annealing S2 at 500 ºC.

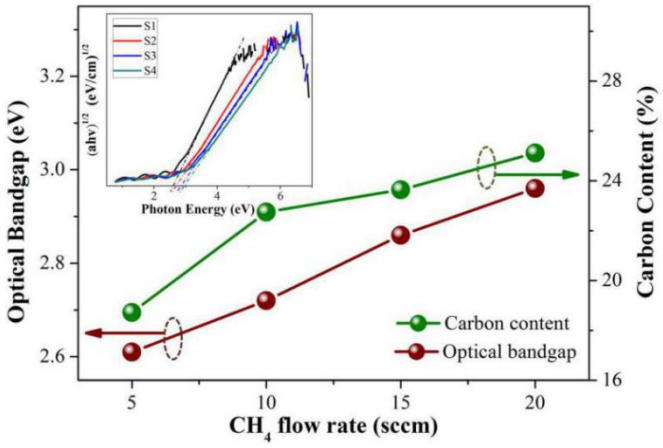


Fig. 6. Optical band gap and C content of a-$SiC_xO_y$ films as a function of $CH_4$ flow rates.

Fig. 6 shows the dependence of the optical band gap ($E_{opt}$) of the films on $CH_4$ flow rates. $E_{opt}$ is calculated from the Tauc plot equation $(\alpha h\nu)^{1/2}=B^{1/2}(h\nu- E_{opt})$, where $\alpha$ is the absorption coefficient and $h\nu$ is the photon energy[15]. $E_{opt}$ increases from 2.6 to 2.9 eV as the $CH_4$ flow rate increases from 5 to 20 sccm. This behavior is closely correlated to the increased C content of the films, as revealed in Fig. 6. To gain more insight on the optical properties of a–$SiC_xO_y$ films, the band characters of SiCO systems and involved point defect were calculated with the sX hybrid function. As shown in Fig. 7(a), the defect-free atomic structure of the amorphous SiCO model was constructed according to the procedures described in the experimental section. The component ratio in the model is close to the component ratio of S4 as measured by the XPS (Table 1).

**Table 1**

| | | Si | O | C | Bandgap(eV) |
|---|---|---|---|---|---|
| S4 | Experiment | 44.83% | 30.06% | 25.11% | 2.9 |
| | Simulation | 45 (44.55%) | 31 (30.69%) | 25 (24.75%) | 2.8 |

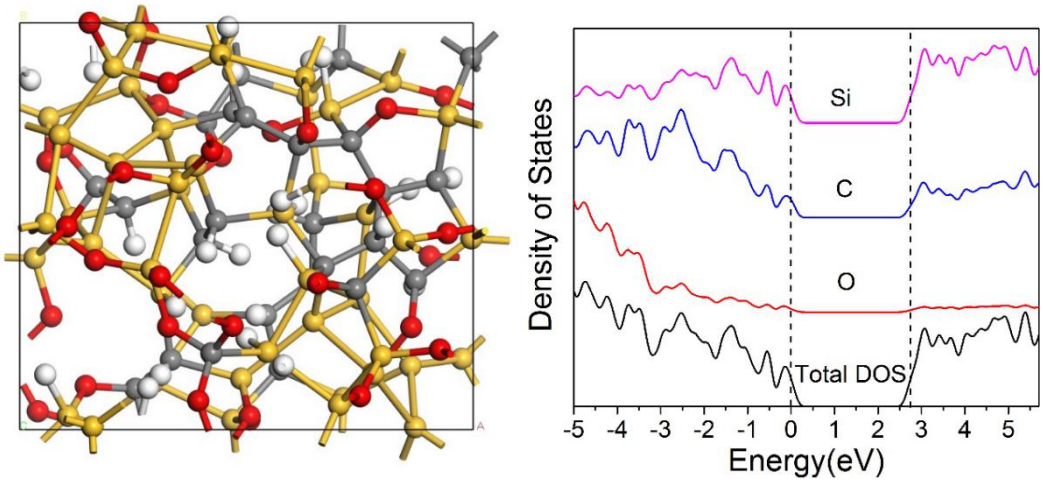


Fig. 7. The amorphous SiCO model (S4) with no defects:(a) the atomic structure , (b) the DOS.

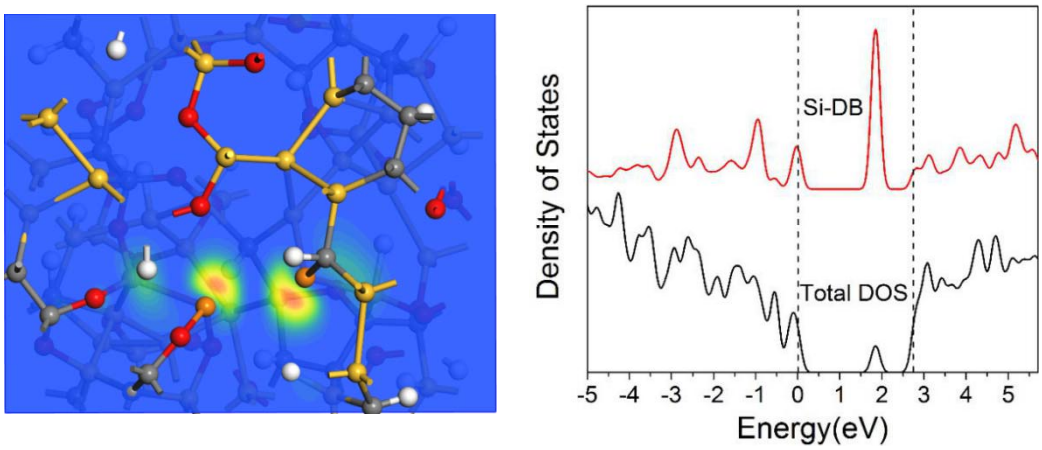


Fig. 8. The S4 model with Si dangling bonds (a) atomic structure and defect orbital; (b) Partial DOS on Si atoms with DBs.

In the model, each atom binds in the correct coordination and no 4-membered ring

appears. The density of states (DOS) of the model, as calculated by the sX exchange correlation functional, is shown in Fig. 7(b). The calculated band gap is 2.8 eV, which is close to the optical band gap (2.9 eV) estimated by the Tauc plot equation (Fig. 6). The DOS figure shows a clean band gap for this defect-free model. Moreover, the valence band edge and conduction band edge are contributed by Si and C atoms. Therefore, the band gap of a–$SiC_xO_y$ is mainly determined by the interaction among Si and C atoms. Thus, the widening of the band gap with increasing $CH_4$ flow rate can be attributed to the replacement of weak Si–Si bonds by stronger Si–C bonds. Fig. 8(a) shows the electronic orbital of the Si dangling bond (DB) defect in the $SiC_xO_y$ system, as given by the sX functional. The defect orbital is highly localized on two 3-fold Si atoms. The partial DOS (Fig. 8(b)) indicates that Si DB defects introduce a mid-gap state at 1.85 eV above the valence band minimum. This result is in good agreement with the PL peak energy observed in S4. Accordingly, the strong light emission of the films can be ascribed to the recombination of excited electrons and holes in Si DB defects. The tunable light emission with the increasing $CH_4$ rate can be attributed to the substitution of stronger Si–C bonds for weak Si–Si bonds.

To measure the optical gain coefficient, the geometry structure of $SiN_x$/a-$SiC_xO_y$ (S4)/$SiO_2$ strip-loaded waveguide were fabricated, and the light emission is detected by VSL technique, as shown in the inset of Fig. 9. Fig. 9 shows the integrated PL intensity of S4 as a function of pump power. The integrated PL intensity is found to rise up with the pumping laser power in a superliner increase manner. This strongly indicates the existence of stimulated emission in the waveguide [35].

Fig. 10 shows the amplified spontaneous emission (ASE) intensity $I_{ASE}$ versus the pumping length from the strip-loaded $SiN_x$/a-$SiC_xO_y$ (S4)/$SiO_2$ waveguide measured at a wavelength of 325nm. One can see that the $I_{ASE}$ tends to increase with increasing the pumping length, as shown in the inset of Fig. 10. For the shorter pumping length (<800um), the $I_{ASE}$ increase exponentially with the pumping length. According to the one-dimensioned amplifier model, $I_{ASE}$ can be expressed by the following equation [36],

$$I_{ASE}(l) = \frac{J_{SP}(\Omega)}{g} \cdot (e^{gl} - l)$$

where $l$ is the pumping length of waveguide, $J_{SP}(\Omega)$ is the spontaneous emission intensity within the small solid angle Ω, g is the net optical gain coefficient. By fitting with the one-dimensioned amplifier equation, the net optical gain coefficient g can be obtained. It is found that the net optical gain coefficient g is about 53.5$cm^{-1}$ at 630 nm,

which shows a comparable gain coefficient to that reported in Ref.[37]. It is the first time to observe the optical gain in a-$SiC_xO_y$ films. Based on the above experimental and theoretical results, three-level luminescent model can be proposed to explain the observed optical gain, as shown in Fig. 11. Under excitation, the electrons from valence band are excited to the high excited state above conduction band and then relax very rapidly to the Si DB defects state. With this model, the population inversion between the Si DB defects radiative states and valence band would contribute to the observed optical gain in our case.

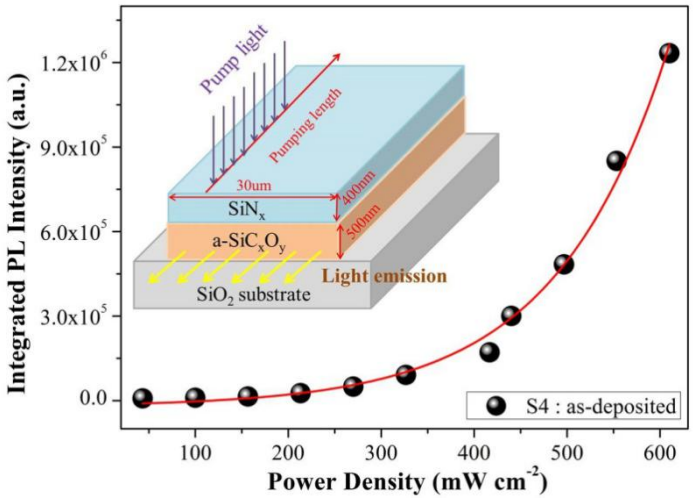


Fig. 9. Pumping power dependence of PL intensity for S4 at an excitation wavelength of 325nm from He-Cd laser. The inset shows the geometry structure of $SiN_x$/a-$SiC_xO_y$ (S4)/$SiO_2$ strip-loaded waveguide.

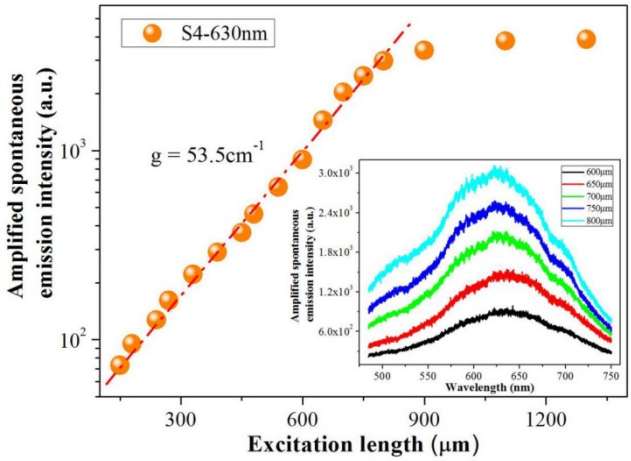


Fig. 10. The ASE intensity at wavelength of 630 nm as a function of the excitation length for S4. The inset shows the PL spectra of waveguide (S4) with different pumping length.

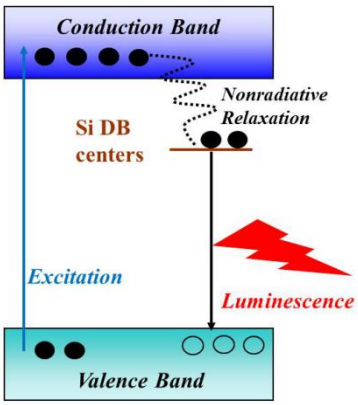


Fig. 11. Schematic three level energy diagram and the exciton recombination processes for a–$SiC_xO_y$ film.

## 4. Conclusions

A series of luminescent $SiC_xO_y$:H films were fabricated by VHF-PECVD technique. HRTEM measurements and Si 2*p* XPS spectra demonstrate that the films are amorphous $SiC_xO_y$ phase structure. The films, which were fabricated at different $CH_4$ flow rates, exhibit strong photoluminescence with tuning from the near-infrared to orange regions. The PL and EPR spectra, as well as the first-principles calculation, reveal that the strong light emission resulted from the recombination of excited electrons and holes in Si DB defects that introduces a mid-gap state in the band gap. The net optical gain coefficient of 53.5$cm^{-1}$ was also demonstrated in a-$SiC_xO_y$, which is explained using a three-level model based on population inversion of radiative states associated with the Si DB defects. The present results demonstrate that the $SiC_xO_y$ system can be a very competitive candidate in the photonic and optoelectronic applications.

## References

[1] J. Robertson, M. J.Powell, Gap states in silicon nitride, Appl. Phys. Lett. 44(1984) 415-417.
[2] L. Pavesi, L. Dal Negro, C. Mazzoleni, G. Franzo, F. Priolo, Optical gain in silicon nanocrystals, Nature 408 (2000) 440-444.
[3] G. R. Lin, Y. H. Pai, C. T. Lin, C. C. Chen, Comparison on the electroluminescence of Si-rich $SiN_x$ and $SiO_x$ based light-emitting diodes, Appl. Phys. Lett. 96 (2010) 263514.
[4] R. Limpens, S. L. Luxembourg, A. W. Weeber, T. Gregorkiewicz, Emission efficiency limit of Si nanocrystals, Sci. Rep. 6 (2016) 19566.

[5] D. Li, F. Wang, D. Yang, Evolution of electroluminescence from silicon nitride light-emitting devices via nanostructural silver, Nanoscale 5 (2013) 3435-3440.
[6] R. Huang, Z. Lin, Z. Lin, C. Song, Y. Guo, X. Wang, J. Song, Suppression of Hole Overflow and Enhancement of Light Emission Efficiency in Si Quantum Dots based Silicon Nitride Light Emitting Diodes, IEEE J Sel. Topics Quantum. Electron. 20 (2014) 8200306.
[7] Y. Guo, Z. Lin, R. Huang, Z. Lin, C. Song, J. Song, X. Wang, Efficiency enhancement for SiN-based light emitting device through introduction of Si nanocones in emitting layer, Opt. Mater. Express, 5 (2015) 969-976.
[8] L. Xu, L. Jin, D. Li, D. Yang, Effects of excess silicon on the 1540 nm $Er^{3+}$ luminescence in silicon rich oxynitride films, Appl. Phys. Lett. 103 (2013) 071101.
[9] P. Zhang, K. Chen, H. Dong, P. Zhang, Z. Fang, W. Li, J. Xu, X. Huang, Higher than 60% internal quantum efficiency of photoluminescence from amorphous silicon oxynitride thin films at wavelength of 470 nm, Appl. Phys. Lett. 105 (2014) 011113.
[10] K. Xu, Q. Yu, G. Li, Increased efficiency of silicon light-emitting device in standard Si-CMOS technology, IEEE J. Quantum Elect. 51 (2015) 1-6.
[11] S. Lin, X. Zhang, P. Zhang, D. Tan, J. Xu, W. Li, K. Chen, High-efficiency near-infrared emission from Bismuth-doped $SiO_{0.73}$ thin films fabricated by ion implantation technology, Opt. Lett. 41 (2016) 630-633.
[12] L. Dal Negro, J. H. Yi, L. C. Kimerling, S. Hamel, A. Williamson, G. Galli, Light emission from silicon-rich nitride nanostructures, Appl. Phys. Lett. 88 (2006) 183103 -183103-3.
[13] R. Huang, J. Song, X. Wang, Y. Q. Guo, C. Song, Z. H. Zheng, X. L. Wu, P. K. Chu, Origin of strong white electroluminescence from dense Si nanodots embedded in silicon nitride, Opt. Lett. 37 (2012) 692–694.
[14] F. Wang, D. Li, D. Yang, D. Que, Tailoring effect of enhanced local electric field from metal nanoparticles on electroluminescence of silicon-rich silicon nitride, IEEE J Sel. Topics Quantum. Electron. 19(2013) 4602504-4602504.
[15] R. Huang, Z. Lin, Y. Guo, C. Song, X. Wang, H. Lin, L. Xu, J. Song and H. Li, Bright red, orange-yellow and white switching photoluminescence from silicon oxynitride films with fast decay dynamics, Opt. Mater. Express. 4 (2014) 205.
[16] X. Wang, R. Huang, C. Song, Y. Guo, and J. Song, Effect of barrier layers on electroluminescence from $Si/SiO_xN_y$ multilayer structures, Appl. Phys. Lett. 102 (2013) 081114.
[17] S. Y. Seo, K. S. Cho, J. H. Shin, Intense blue–white luminescence from carbon-doped silicon-rich silicon oxide, Appl. Phys. Lett. 84 (2004) 717-719.
[18] Y. Ding, H. Shirai, White light emission from silicon oxycarbide films prepared by using atmospheric pressure microplasma jet, J. Appl. Phys. 105 (2009) 043515.
[19] Z. Lin, Y. Guo, C. Song, J. Song, X. Wang, Y. Zhang, R. Huang. Influence of the oxygen content in obtaining tunable and strong photoluminescence from low-temperature grown silicon oxycarbide films, J. Alloys Compd. 633 (2015) 153-156.
[20] S. Gallis, M. Huang, A. E. Kaloyeros, Efficient energy transfer from silicon oxycarbide matrix to Er ions via indirect excitation mechanisms, Appl. Phys. Lett. 90

(2007) 161914.
[21] S. Boninelli, G. Bellocchi, G. Franzò, M. Miritello, F. Iacona, New strategies to improve the luminescence efficiency of Eu ions embedded in Si-based matrices J. Appl. Phys. 113 (2013) 143503.
[22] Z. Lin, R. Huang, H. Wang, Y. Wang, Y. Zhang, Y. Guo, J. Song, C. Song, H. Li, Dense nanosized europium silicate clusters induced light emission enhancement in Eu-doped silicon oxycarbide films, J. Alloys Compd. 694 (2017) 946-951.
[23] S. Gallis, V. Nikas, H. Suhag, M. Huang, A. E. Kaloyeros, White light emission from amorphous silicon oxycarbide (a-$SiC_xO_y$) thin films: Role of composition and postdeposition annealing, Appl. Phys. Lett. 97 (2010) 081905.
[24] G. Bellocchi, F. Iacona, M. Miritello, T. Cesca and G. Franzò, SiOC thin films: an efficient light source and an ideal host matrix for $Eu^{2+}$ ions, Opt. Express 21 (2013) 20280.
[25] Z. Lin, Y. Guo, J. Song, Y. Zhang, C. Song, X. Wang, R. Huang, Effect of thermal annealing on the blue luminescence of amorphous silicon oxycarbide films, J. Non-Cryst. Solids 428 (2015) 184-188.
[26] V. Nikas, S. Gallis, M. Huang, A. E. Kaloyeros, A. P. D. Nguyen, A. Stesmans, V. V. Afanasev, The origin of white luminescence from silicon oxycarbide thin films, Appl. Phys. Lett. 104 (2014) 061906.
[27] Z. Chen, Y. Wang, Y. Zou, J. Wang, Y. Li, H. Zhang, Origin of the blue photoluminescence from $SiO_2$ (SiC)/SiC on Si substrate, Appl. Phys. Lett. 89 (2006) 141913.
[28] H. Kato, N. Kashio, Y. Ohki, K. Seol, T. Noma, Band-tail photoluminescence in hydrogenated amorphous silicon oxynitride and silicon nitride films, J. Appl. Phys. 93 (2003) 239-244.
[29] P. Xue, D. Pei, H. Zheng, W. Li, V. Afanas'ev, M. Baklanov, J. Marneffe, Y. Lin, H. Fung, C. Chen, Y. Nishi, J. Shohet, The effects of vacuum-ultraviolet radiation on defects in low-k organosilicate glass (SiCOH) as measured with electron-spin resonance, Thin Solid Films 616 (2016) 23-26.
[30] E. N. Kalabukhova, S. N. Lukin, D. V. Savchenko, B. D. Shanina, A. V. Vasin, V. S. Lysenko, A. N. Nazarov, A. V. Rusavsky, J. Hoentsch, Y. Koshka, EPR study of carbon and silicon related defects in carbon-rich hydrogenated amorphous silicon-carbon films, Phys. Rev. B 81 (2010) 155319.
[31] D. K. Basa, G. Ambrosone, U. Coscia, A. Setaro, Crystallization of hydrogenated amorphous silicon carbon films with laser and thermal annealing, Appl. Surf. Sci. 255 (2009) 5528.
[32] S. Gallis, V. Nikas, M. Huang, E. Eisenbraun, and A. E. Kaloyeros, Comparative study of the effects of thermal treatment on the optical properties of hydrogenated amorphous silicon-oxycarbide, J. Appl. Phys. 102 (2007) 024302.
[33] A. Grill, Plasma enhanced chemical vapor deposited SiCOH dielectrics: from low-k to extreme low-k interconnect materials, J. Appl. Phys. 93 (2003) 1785.
[34] C. Song, R. Huang, X. Wang, Y. Guo, J. Song, Y. Zhang, Z. Zheng, Effects of hydrogen on photoluminescence properties of a-$SiN_x$:H films prepared by VHF-PECVD, Appl. Surf. Sci. 258 (2011) 1290.

[35] Q. H. Song, L. Y. Liu, S. M. Xiao, X. C. Zhou, W. C. Wang, L. Xu, Unidirectional high intensity narrow-linewidth lasing from a planar random microcavity laser, Phys. Rev. Lett. 96 (2006) 033902.
[36] J. Zhu, X. Wu, M. Zhang, Y. Wang, X. Ning, Y. Zhao, M. Lu, Photoluminescence responses of Si nanocrystal to differing pumping conditions, J. Appl. Phys. 110 (2011) 013502.
[37] D. C. Wang, H. C. Hao, J. R. Chen, C. Zhang, J. Zhou, J. Sun, M. Lu, White light emission and optical gains from a Si nanocrystal thin film, Nanotechnology 26 (2015) 475203.